Published in final edited form as:
Angew Chem Int Ed Engl. 2014 August 4; 53(32): 8406–8410. doi:10.1002/anie.201404519.

Synthesis of Tantalum Oxide Nanoparticles for Imaging Articular Cartilage Using X-Ray Computed Tomography: Visualization of Ex vivo/In vivo Murine Tibia and Ex vivo Human Index Finger Cartilage**

Jonathan D. Freedman,
Departments of Biomedical Engineering, Chemistry and Pharmacology, Boston University, Boston, MA 02115 (USA), Homepage: http://people.bu.edu/mgrin/

Dr. Hrvoje Lusic,
Departments of Biomedical Engineering, Chemistry and Pharmacology, Boston University, Boston, MA 02115 (USA), Homepage: http://people.bu.edu/mgrin/

Prof. Brian D. Snyder, and
Center for Advanced Orthopaedic Studies, Beth Israel Deaconess Medical Center, Harvard Medical School, Boston, MA 02115 (USA)

Prof. Mark W. Grinstaff
Departments of Biomedical Engineering, Chemistry and Pharmacology, Boston University, Boston, MA 02115 (USA), Homepage: http://people.bu.edu/mgrin/

Brian D. Snyder: Brian.Snyder@childrens.harvard.edu; Mark W. Grinstaff: mgrin@bu.edu

Abstract

Tantalum oxide (Ta_2O_5) nanoparticles are used as X-ray contrast media for micro computed tomography (μCT) imaging of articular cartilage. The cationic nanoparticles are attracted to the anionic glycosaminoglycans in the cartilage tissue.

Keywords

Nanoparticles; Imaging; CECT; X-ray; Cartilage

Nanoparticles (NPs) display distinct properties apart from individual atoms or bulk material as a consequence of their composition, small diameter, high surface area, and confined electronic structure.[1] In medicine, NPs are currently investigated as delivery vehicles for pharmacologically active agents,[2] as reagents for diagnostic assays,[3] as biosensors,[4] and as imaging contrast agents for MRI, fluorescence, PET, and X-ray.[5] With regards to the

**The authors gratefully acknowledge support in part from the National Institutes of Health (R01GM098361), the T32 Pharmacology Training grant (5T32GM008541-14), and Boston University. We would also like to acknowledge the Center for Advanced Orthopaedic Studies at Beth Israel Deaconess Medical Center for use of their μCT scanner.

Correspondence to: Mark W. Grinstaff, mgrin@bu.edu.

Supporting information for this article is available on the WWW under http://www.angewandte.org or from the author.

latter, NPs containing gold, bismuth, and tantalum are used as X-ray contrast media for contrast enhanced computed tomography (CECT) to image lymph nodes[6] and the vascular system.[7] Tantalum is an attractive contrast agent material for CT imaging because it has a higher *k*-edge (67.4 keV) than conventional iodinated contrast agents (*k*-edge 33.2 keV) and thus absorbs a greater fraction of the X-rays produced at clinical scanning voltages (80–140 keV). The higher *k*-edge also decreases low energy filtration and lessens beam hardening artifacts. In addition, tantalum NPs are biocompatible and have been used successfully in murine *in vivo* imaging models.[6, 7c–e, 8] Commonly, tantalum is incorporated in the form of core-shell tantalum oxide (Ta_2O_5) NPs, where the radiopaque Ta_2O_5 core is surrounded by functionalized silane ligands. This class of NPs has facile methods to modify the surface and produces stable, low viscosity nanoparticle suspensions at aqueous physiological conditions. Given our interest in imaging articular cartilage – the smooth, hydrated tissue that lines the ends of bones in load bearing joints – to ascertain the thickness, morphology, and biochemical state, we are designing Ta_2O_5 NPs as contrast agents for imaging cartilage. Herein, we report the synthesis and characterization of phosphonate (**1**), ammonium (**2**), and carboxylate (**3**) functionalized core-shell Ta_2O_5 NPs, the imaging of *ex vivo* and *in vivo* murine cartilage, the kinetics of NP penetration into cartilage as a function of surface charge, and the detection of an osteoarthritic defect in a human cadaver metacarpal phalangeal (MCP) joint.

Articular cartilage is a three dimensional collagen (10–20% by wt)[9] matrix that readily absorbs water (68–85% by wt). The hydrated state of articular cartilage is maintained by heavily sulfated and carboxylated glycosaminoglycans (GAGs, 5–10% by wt) that grant cartilage a fixed negative charge. The loss of GAGs in cartilage is a sign of disease,[10] and correlates to worsening mechanical properties[11] and further degradation of the joint soft tissues and bone. Thus, imaging methods using targeted contrast agents that evaluate changes in *ex vivo* or *in vivo* cartilage or bone are of interest.[12] For cartilage, measurements of thickness, morphology, and/or GAG content are useful for assessing joint health and diagnosing diseases such as osteoarthritis (OA).[12b–d, 13] We hypothesize that ammonium functionalized, positively charged Ta_2O_5 NPs (**2**) will accumulate in and provide higher-contrast images of the articular cartilage tissue as a consequence of the fixed-negative charge of the GAGs, compared to the neutral (**1**) or negatively (**3**) charged Ta_2O_5 NPs (see Scheme 1 and Figure SI-1).

To investigate the effects of different surface charges, Ta_2O_5 NPs were synthesized possessing different terminal functional groups – phosphonate (neutral; **1**), ammonium (cationic; **2**), and carboxylate (anionic; **3**) (Scheme 1). The synthetic procedure was adapted from Hyeon[6] and Bonitatibus.[7e] (See the Experimental Section for details). Briefly, the Ta_2O_5 core was formed by hydrolysis of tantalum ethoxide, $Ta(OEt)_5$; the size of the NPs was controlled by the amount of water and isobutyric acid added in *n*-propanol. The silane ligands were subsequently coupled to the NP surface in *n*-propanol under reflux conditions. In the case of NPs **2** and **3**, the final product was obtained following removal of the protecting groups. ^1H & ^{13}C NMR analysis showed characteristic broad peaks[7e] that were consistent with the respective ligand for each NP type (Figure SI-2–4). The FTIR spectrum of NP **2** possessed a characteristic ammonium cation absorption band at 2919 cm^{-1} (Figure

SI-5). Transmission electron microscopy (EM) revealed particles between 5–10 nm in diameter (Figure SI-6c). Sizing by scanning EM (Figure 1 and Figure SI-6a) was in approximate agreement with dynamic light scattering (DLS) results (Table SI-1, D±S.D.: NP **1** = 6.5±0.5, NP **2** = 3.3±0.7, NP **3** = 5.0±0.3). Zeta potential measurements revealed distinct charges for each of the NP types (**1**: −1.14 mV, **2**: +7.58 mV, **3**: −19.07 mV; in pH 7.4).

To evaluate the NP contrast media ability to image articular cartilage, we serially imaged murine *ex vivo* proximal tibial cartilage of the knee joint after immersion in a solution of NPs **1**, **2**, & **3**. This cartilage comprises the distal part of the knee joint and is commonly evaluated in murine OA models.[14] Contrast media concentrations of 40 mg NP/mL were chosen based on a pilot imaging experiment showing sufficient attenuation for cartilage imaging and based on the desired signal strength of known small molecule iodinated CT contrast agents (Figure SI-7).[12b] The osmolality of the solutions was balanced to 400 mOsm to match the ionic strength of synovial fluid.[15] As shown in Figure 2, uptake of NP **2** was faster and significantly greater than NPs **1** ($p < 0.0001$), or **3** ($p < 0.0001$), as measured after 48 hours of incubation. An exponential function was fit for the data obtained with NP **2** ($f(t)= \alpha\ (1-e^{-t/\tau})$; $\tau = 7.5$ hr) showing that diffusion leveled out (> 95% of equilibrium) after 24 hours. NPs **1** and **3** showed slow linear diffusion trends into the cartilage tissue and produced < 200 change in HU over 48 hours of immersion. The results from the quantitative uptake studies can be visualized, as uptake of NP **2** provides good visualization of the tibial cartilage in agreement with areas of histological images stained with Safranin-O, a standard stain used to mark GAGs in cartilage tissue (Figure SI-9b). NP **2** distributed into the entirety of the articular cartilage increasing the attenuation and enabling clear visual delineation of cartilage from both air and bone. In addition, NP **2** also diffused into soft tissue remnants near the tendon insertion sites and were visualized by CECT. NPs **1** and **3** were seen to accumulate at the surface, were largely excluded from the cartilage, and did not produce definitive cartilage-air or cartilage-bone interfaces (Figure 3).

Next, CECT with NP **2** was used to image a naturally occurring cadaveric osteoarthritic defect in the proximal MCP joint of a human index finger of a 73-year old male. This type of defect is commonly seen due to overuse, such as typing or texting, and is also associated with advanced age and injury.[16] The joint was baseline imaged and then immersed in 40 mg NP/mL of NP **2** for 24 hours and then re-imaged. In baseline 3D and 2D CT images, the overall attenuation of cartilage is low and the boundaries between bone, cartilage, and air are poorly resolved (Figure 4: A, D, F). On the other hand, the contrast enhanced images exhibited high attenuation and showed penetration of NP **2** into in the areas of roughened cartilage and the defect could be clearly visualized (Figure 4: B, E, G). In the sample imaged, the large defect closely matched the area of exposed bone and irregular cartilage edges as seen on gross inspection after disarticulation (Figure 4C).

In areas of the MCP joint where the cartilage tissue was intact, NP **2** accumulated throughout the tissue but was concentrated at the surface of the cartilage. The penetration of NP **2** in human cartilage appears to be different than in mouse cartilage, and this may be a consequence of the different cartilage pore sizes or compositional differences. Nonetheless,

contrast agents that analyze the surface morphology of articular cartilage and surrounding soft tissue are useful to detect defects such as cartilage lesions[13b] and labrum tears.[17]

NP **2** possesses a positive charge and in general, positively charged NPs are more cytotoxic than neutral materials.[18] Our preliminary assessment agrees with this as NPs **2** and **3** exhibited moderate cytotoxicity (80-60%) against 3T3 fibroblasts after 4 hours (Figure SI-11) and the results were comparable to ioxaglate, an FDA approved and clinically used iodinated CT agent, in this assay (Figure SI-12). Given this result, we further optimized the NP surface coating to contain (short) polyethylene glycol (PEG) ligands and a tetra-ammonium group (1:1), where the ammonium group ensures a cationic charge and the PEG reduces cytotoxicity (NP **4**; Figure 5). NP **4** exhibits an improved cytotoxicity profile compared to NP **2**, and is non-cytotoxic being similar to the untreated control (Figure SI-13). NP **4** allows visualization of *ex vivo* cartilage similar to NP **2** (Figure SI-13b). Intravenous injection of NP **4** (1 mL of 40 mg/mL) showed high contrast in the calyces of the kidneys after 15 minutes suggesting renal clearance and no accumulation in the liver or spleen. This result is consistent with nanoparticles of this size.[19] This delivery route was chosen over intra-articular injection to ensure sufficient material for CT imaging.

To demonstrate *in vivo* feasibility, NP **4** was injected intra-articularly into the knee of an adult male Wistar rat (100 μL of 40 mg/mL). This delivery approach ensures a high concentration of contrast agent in the local cartilage area and minimizes systemic exposure, while requiring less injected material compared to an IV injection to obtain the same contrast agent concentration in the joint. This procedure (arthrography) is currently performed clinically with iodinated CT contrast agents for imaging of the cartilage. The knee was flexed five times to facilitate diffusion of the contrast agent throughout the joint and scanned by low-resolution pQCT (100 μm^2 in plane). In a composite colorized axial CT image, showing the bone in grayscale, the contrast can be seen in green throughout the joint space and concentrated at specific cartilage regions at the bone interface (Figure 6A). A similar *in vivo* result was observed with the other cationic NP, NP **2** (Figure SI-14). After *in vivo* imaging, the rat was allowed to recover and displayed no signs of distress. The rat was then immediately sacrificed and the joint scanned by high-resolution μCT (36 μm^3 isotropic). Similarly, the equivalent *ex vivo* axial image shows contrast throughout the joint as well as penetrating and throughout the cartilage (Figure 6B). The cartilage is easier seen in the coronal view shown in Figure 6C, where the cartilage (green) is between the bone and synovial space. Subsequent histological examination of the cartilage revealed no adverse effects and the results were similar to untreated control cartilage.

Ta_2O_5 NPs with significant differences in overall surface charges were synthesized and evaluated as CT contrast media for imaging of murine and human articular cartilage. The positively charged NP exhibited substantially greater affinity for articular cartilage, due to the favorable Coulombic attraction[12b, 20] to the fixed, negatively charged GAGs of the cartilage. Moreover, by maintaining the positive charge on the NP surface and introducing a PEG coating, a NP formulation, **4**, is described for successful *in vivo* cartilage imaging. These results demonstrate the importance of electrostatic based targeting and transport for nano-sized material into articular cartilage, and the successful μCT imaging of *ex vivo* and *in vivo* imaging of articular cartilage with nanoparticulate cationic contrast agents.

Furthermore, these findings support the use and further development of μCT imaging (instruments, contrast agents, software) for small animal models to provide both quantitative and 3D spatial assessment of cartilage, which have conventionally been assessed qualitatively with 2D histology and precluded from MR imaging due to resolution limitations. Such tools are immediately of interest for preclinical evaluation of pharmacological agents, biologics, and tissue engineering strategies for the treatment of osteoarthritis and for the future development of CT agents to assist in the diagnosis of osteoarthritis in the clinic.

Experimental Section

Ethyl phosphonate tantalum oxide NPs (1)

The NPs were synthesized according to the literature procedure.[7e] ^{1}H NMR (400 MHz, D_2O): δ =0.69 (br s, 2 H), 1.19 (br s, 3 H), 1.72 (br s, 2 H), 4.00 (br s, 2 H). ^{31}P NMR (162 MHz, D_2O): δ = 36.3 (br s). FTIR (cm^{-1}): 1444 (weak), 1412 (weak), 1273 (weak), 1215 (strong), 1165 (medium), 1094 (weak), 1020 (very strong), 938 (very strong), 777 (strong). ICP-AES: Ta/Si (wt/wt) 2.08 ± 0.02.

(*n*-Propylamine HCl salt) tantalum oxide NPs (2)

Isobutyric acid (0.44 mL) and D_2O (0.5 mL) were added to an *n*-propanol (34 mL) solution. Tantalum(V) ethoxide (1.87 g, 1.19 mL) was added dropwise at a rate of 0.2 mL/min, and the solution was left to stir for 16 h at rt, under N_2 atmosphere. The solution was then diluted by addition of *n*-propanol (20 mL), followed by addition of *tert*-butyl 3-(triethoxysilyl)propylcarbamate (5 g) in *n*-propanol (15 mL) at a rate of 1 mL/min. The reaction was subsequently refluxed for 2 h, and then cooled to rt. Next, NH_4OH (0.1 M, 250 mL) was added to the solution, and the reaction was stirred for 16 h at rt. Subsequently, H_2O (40 mL), and aq. HCl (1.2 M, 10 mL) were added to the flask dropwise over 20 min. The reaction was then allowed to proceed at 50 °C for 48 h. The reaction was cooled to rt, and filtered through a 0.22 μm membrane, and the volatiles were evaporated. The residue was redissolved in MeOH (50 mL), and cooled to 0 °C. A solution of 2 N HCl (50 mL) was added to the flask and the reaction was stirred at rt for 48 h. The solution was neutralized to pH 7 by addition of Na_2CO_3, filtered through a 0.22 μm membrane, and then transferred into dialysis tubing (MWCO 3.5 kDa). The product was dialyzed over 72 h, with frequent water changes. Removal of volatiles by lyophilization afforded **2** as white powder. ^{1}H NMR (400 MHz, D_2O): δ =0.53 (br s, 2 H), 1.64 (br s, 2 H), 2.89 (br s, 2 H). ^{13}C NMR (100 Hz, D_2O): δ = 9.7, 21.0, 41.7. FTIR (cm^{-1}): 3320 (weak), 2919 (very strong), 1611 (medium), 1502 (medium), 1210 (weak), 1044 (weak), 922 (strong), 802 (weak). ICP-AES: Ta/Si (wt/wt) 4.96 ± 0.06.

Sodium propanoate tantalum oxide NPs (3)

Isobutyric acid (0.44 mL) and D_2O (0.5 mL) were added to an *n*-propanol (34 mL) solution. Tantalum(V) ethoxide (1.87 g, 1.19 mL) was added dropwise at a rate of 0.2 mL/min, and the solution was left to stir for 16 h at rt, under N_2 atmosphere. The solution was diluted by addition of *n*-propanol (20 mL), followed by addition of methyl 3-(triethoxysilyl)propanoate (5 g) in *n*-propanol (15 mL) at a rate of 1 mL/min. The reaction was subsequently refluxed

for 2 h, and then cooled to rt. Next, NH_4OH (0.1 M, 250 mL) was added to the solution, and the reaction was stirred for 16 h at rt. Subsequently, H_2O (40 mL), and aq. HCl (1.2 M, 10 mL) were added to the flask dropwise over 20 min. The reaction was then allowed to proceed at 50 °C for 48 h. The reaction was cooled to rt, and filtered through a 0.22 μm membrane, and the volatiles were evaporated. The residue was redissolved in MeOH (50 mL), and cooled to 0 °C. DI water (50 mL) was added the flask, and the pH was adjusted to pH 10, by addition of Na_2CO_3 and the reaction was stirred at 40 °C for 48 h. The solution was neutralized to pH 7 by addition of 1 N HCl, filtered through a 0.22 μm membrane, and then transferred into dialysis tubing (MWCO 3.5 kDa). The product was dialyzed over 72 h, with frequent water changes. Removal of volatiles by lyophilization afforded **3** as white powder. ^{1}H NMR (400 MHz, D_2O): δ =0.59 (br s, 2 H), 2.00 (br s, 2 H). ^{13}C NMR (100 Hz, D_2O): δ = 9.2, 30.6, 185.8. FTIR (cm^{-1}): 3265 (weak), 2927 (weak), 1656 (weak), 1562 (strong), 1410 (strong), 1304 (weak), 1187 (weak), 1033 (medium), 912 (very strong). ICP-AES: Ta/Si (wt/wt) 2.64 ± 0.05.

Tetra-ammonium-PEG Tantalum Oxide NPs (4)

Isobutyric acid (0.44 mL) and D_2O (0.5 mL) were added to an *n*-propanol (34 mL) solution. Tantalum(V) ethoxide (1.87 g, 1.19 mL) was added dropwise at a rate of 0.2 mL/min, and the solution was left to stir for 16 h at rt, under N_2 atmosphere. The solution was then diluted by addition of *n*-propanol (20 mL), followed by addition of a mixture of *N*-trimethoxylsilylpropyl-*N*,*N*,*N*-trimethylammonium chloride (2.5 g) and 2-[Methoxyl(polyethyleneoxy)propyl]trimethoxylsilane (2.5 g) in *n*-propanol (15 mL) at a rate of 1 mL/min. The reaction was subsequently refluxed for 2 h, and then cooled to rt. Next, NH_4OH (0.1 M, 250 mL) was added to the solution, and the reaction was stirred for 16 h at rt. Subsequently, H_2O (40 mL), and aq. HCl (1.2 M, 10 mL) were added to the flask dropwise over 20 min. The reaction was then allowed to proceed at 50 °C for 48 h. The solution was neutralized to pH 7 by addition of Na_2CO_3, filtered through a 0.22 μm membrane, and then transferred into dialysis tubing (MWCO 3.5 kDa). The product was dialyzed over 72 h, with frequent water changes. Removal of volatiles by lyophilization afforded **4** as white powder. ^{1}H NMR (400 MHz, D_2O): δ =0.10 (br s), 1.15 (br s), 1.37 (br s), 2.5–3.3 (br m). FTIR (cm^{-1}): 2871 (strong), 1647 (medium), 1479 (medium). ICP-AES: Ta/Si (wt/wt) 5.18 ± 0.04.

Supplementary Material

Refer to Web version on PubMed Central for supplementary material.

References

1. Roduner E. Chem Soc Rev. 2006; 35:583–592. [PubMed: 16791330]
2. Wanakule P, Roy K. Curr Drug Metab. 2012; 13:42–49. [PubMed: 22385534]
3. Larguinho M, Baptista PV. J Proteomics. 2012; 75:2811–2823. [PubMed: 22119545]
4. Somers RC, Bawendi MG, Nocera DG. Chem Soc Rev. 2007; 36:579–591. [PubMed: 17387407]
5. a) Vivero-Escoto JL, Huxford-Phillips RC, Lin W. Chem Soc Rev. 2012; 41:2673–2685. [PubMed: 22234515] b) Lee N, Choi SH, Hyeon T. Adv Mater. 2013; 25:2641–2660. [PubMed: 23553799] c) Shilo M, Reuveni T, Motiei M, Popovtzer R. Nanomed. 2012; 7:257–269.d) Lusic H, Grinstaff MW. Chem Rev. 2013; 113:1641–1666. [PubMed: 23210836] e) Lee N, Hyeon T. Chem Soc Rev.

2012; 41:2575–2589. [PubMed: 22138852] f) Louie A. Chem Rev. 2010; 110:3146–3195. [PubMed: 20225900] g) Dreaden EC, Alkilany AM, Huang X, Murphy CJ, El-Sayed MA. Chem Soc Rev. 2012; 41:2740–2779. [PubMed: 22109657]

6. Oh MH, Lee N, Kim H, Park SP, Piao Y, Lee J, Jun SW, Moon WK, Choi SH, Hyeon T. J Am Chem Soc. 2011; 133:5508–5515. [PubMed: 21428437]
7. a) Au JT, Craig G, Longo V, Zanzonico P, Mason M, Fong Y, Allen PJ. AJR Am J Roentgenol. 2013; 200:1347–1351. [PubMed: 23701074] b) Rabin O, Manuel Perez J, Grimm J, Wojtkiewicz G, Weissleder R. Nat Mater. 2006; 5:118–122. [PubMed: 16444262] c) Torres AS, Bonitatibus PJ Jr, Colborn RE, Goddard GD, FitzGerald PF, Lee BD, Marino ME. Invest Radiol. 2012; 47:578–587. [PubMed: 22836312] d) Bonitatibus PJ Jr, Torres AS, Kandapallil B, Lee BD, Goddard GD, Colborn RE, Marino ME. ACS Nano. 2012; 6:6650–6658. [PubMed: 22768795] e) Bonitatibus PJ Jr, Torres AS, Goddard GD, FitzGerald PF, Kulkarni AM. Chem Commun. 2010; 46:8956–8958.f) Xiao Q, Bu W, Ren Q, Zhang S, Xing H, Chen F, Li M, Zheng X, Hua Y, Zhou L, Peng W, Qu H, Wang Z, Zhao K, Shi J. Biomaterials. 2012; 33:7530–7539. [PubMed: 22840224]
8. Lee N, Cho HR, Oh MH, Lee SH, Kim K, Kim BH, Shin K, Ahn TY, Choi JW, Kim YW, Choi SH, Hyeon T. J Am Chem Soc. 2012; 134:10309–10312. [PubMed: 22676237]
9. VCH; Mow, R. Basic Orthopaedic Biomechanics and Mechano-Biology. 3. Lippincott Williams & Wilkins; Philadelphia: 2005.
10. Felson DT, Lawrence RC, Dieppe PA, Hirsch R, Helmick CG, Jordan JM, Kington RS, Lane NE, Nevitt MC, Zhang Y, Sowers M, McAlindon T, Spector TD, Poole AR, Yanovski SZ, Ateshian G, Sharma L, Buckwalter JA, Brandt KD, Fries JF. Ann Intern Med. 2000; 133:635–646. [PubMed: 11033593]
11. Lakin BA, Grasso DJ, Shah SS, Stewart RC, Bansal PN, Freedman JD, Grinstaff MW, Snyder BD. Osteoarthr Cartilage. 2013; 21:60–68.
12. a) Parkesh R, Gowin W, Lee TC, Gunnlaugsson T. Org Biomol Chem. 2006; 4:3611–3617. [PubMed: 16990936] b) Joshi NS, Bansal PN, Stewart RC, Snyder BD, Grinstaff MW. J Am Chem Soc. 2009; 131:13234–13235. [PubMed: 19754183] c) Silvast TS, Kokkonen HT, Jurvelin JS, Quinn TM, Nieminen MT, Toyras J. Phys Med Biol. 2009; 54:6823–6836. [PubMed: 19864699] d) Palmer AW, Guldberg RE, Levenston ME. Proc Natl Acad Sci U S A. 2006; 103:19255–19260. [PubMed: 17158799] e) Yin M, Shen J, Pflugfelder GO, Mullen K. J Am Chem Soc. 2008; 130:7806–7807. [PubMed: 18512911] f) Winalski CS, Shortkroff S, Schneider E, Yoshioka H, Mulkern RV, Rosen GM. Osteoarthr Cartilage. 2008; 16:815–822.
13. a) Kokkonen HT, Jurvelin JS, Tiitu V, Toyras J. Osteoarthr Cartilage. 2011; 19:295–301.b) Hirvasniemi J, Kulmala KA, Lammentausta E, Ojala R, Lehenkari P, Kamel A, Jurvelin JS, Toyras J, Nieminen MT, Saarakkala S. Osteoarthr Cartilage. 2013; 21:434–442.c) van Tiel J, Siebelt M, Waarsing JH, Piscaer TM, van Straten M, Booij R, Dijkshoorn ML, Kleinrensink GJ, Verhaar JA, Krestin GP, Weinans H, Oei EH. Osteoarthr Cartilage. 2012; 20:678–685.d) Kulmala KA, Korhonen RK, Julkunen P, Jurvelin JS, Quinn TM, Kroger H, Toyras J. Med Eng Phys. 2010; 32:878–882. [PubMed: 20594900] e) Yoo HJ, Hong SH, Choi JY, Lee IJ, Kim SJ, Choi JA, Kang HS. Radiology. 2011; 261:805–812. [PubMed: 21940505] f) Bansal PN, Joshi NS, Entezari V, Grinstaff MW, Snyder BD. Osteoarthr Cartilage. 2010; 18:184–191.g) Bansal PN, Joshi NS, Entezari V, Malone BC, Stewart RC, Snyder BD, Grinstaff MW. J Orthop Res. 2011; 29:704–709. [PubMed: 21437949] h) Bansal PN, Stewart RC, Entezari V, Snyder BD, Grinstaff MW. Osteoarthr Cartilage. 2011; 19:970–976.i) Hayward LN, de Bakker CM, Gerstenfeld LC, Grinstaff MW, Morgan EF. J Orthop Res. 2012j) Stewart RC, Bansal PN, Entezari V, Lusic H, Nazarian RM, Snyder BD, Grinstaff MW. Radiology. 2013; 266:141–150. [PubMed: 23192774]
14. a) Kotwal N, Li J, Sandy J, Plaas A, Sumner DR. Osteoarthr Cartilage. 2012; 20:887–895.b) Botter SM, van Osch GJ, Clockaerts S, Waarsing JH, Weinans H, van Leeuwen JP. Arthritis Rheum. 2011; 63:2690–2699. [PubMed: 21360519] c) de Hooge ASK, van de Loo FAJ, Bennink MB, Arntz OJ, de Hooge P, van den Berg WB. Osteoarthr Cartilage. 2005; 13:66–73.
15. Baumgarten M, Bloebaum RD, Ross SDK, Campbell P, Sarmiento A. Journal of Bone and Joint Surgery-American Volume. 1985; 67A:1336–1339.
16. Williams FMK, Spector TD. Medicine (Baltimore). 2006; 34:364–368.
17. Yamamoto Y, Tonotsuka H, Ueda T, Hamada Y. Arthroscopy. 2007; 23:1290–1294. [PubMed: 18063172]

18. a) Bhattacharjee S, Rietjens IM, Singh MP, Atkins TM, Purkait TK, Xu Z, Regli S, Shukaliak A, Clark RJ, Mitchell BS, Alink GM, Marcelis AT, Fink MJ, Veinot JG, Kauzlarich SM, Zuilhof H. Nanoscale. 2013b) Soenen SJ, De Cuyper M. Contrast Media Mol Imaging. 2009; 4:207–219. [PubMed: 19810053]

19. Longmire M, Choyke PL, Kobayashi H. Nanomed. 2008; 3:703–717.

20. a) Byun S, Tortorella MD, Malfait AM, Fok K, Frank EH, Grodzinsky AJ. Arch Biochem Biophys. 2010; 499:32–39. [PubMed: 20447377] b) Bajpayee AG, Wong CR, Bawendi MG, Frank EH, Grodzinsky AJ. Biomaterials. 2014; 35:538–549. [PubMed: 24120044]

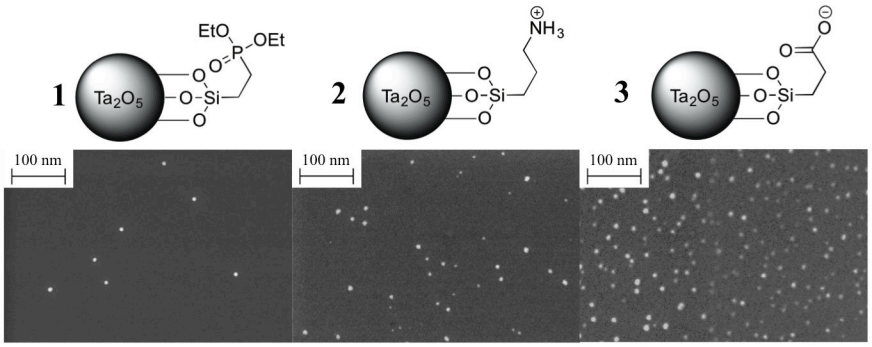

Figure 1.

SEM images of Ta_2O_5 NPs with three different silane ligands. D±S.D.: NP **1** = 7.3±2.9, NP **2** = 6.0±4.4, NP **3** = 9.6±3.3.

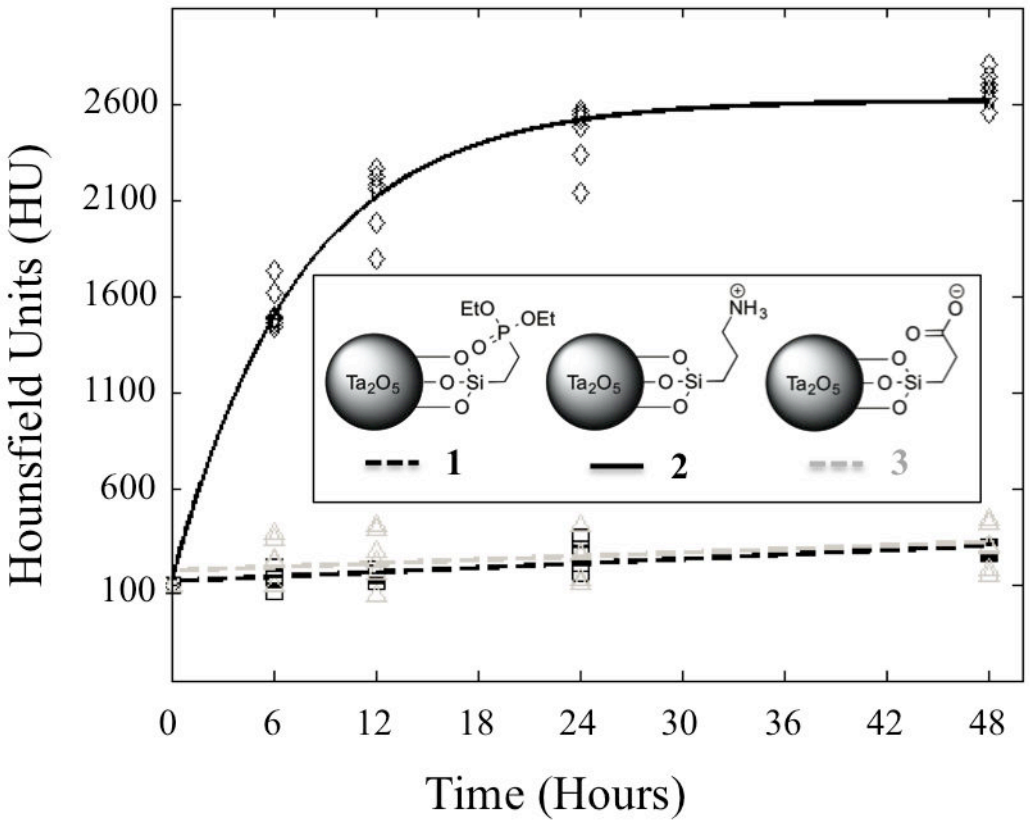

Figure 2.

Diffusion of NP contrast agents into mouse tibia over 48 hours. Solid lines represent fitted data. NP **2** (solid black line) produces greater attenuation than NPs **1** (dashed black line) or **3** (dashed grey line) and diffuses into the cartilage in approximately 24 hours (> 95% of equilibrium).

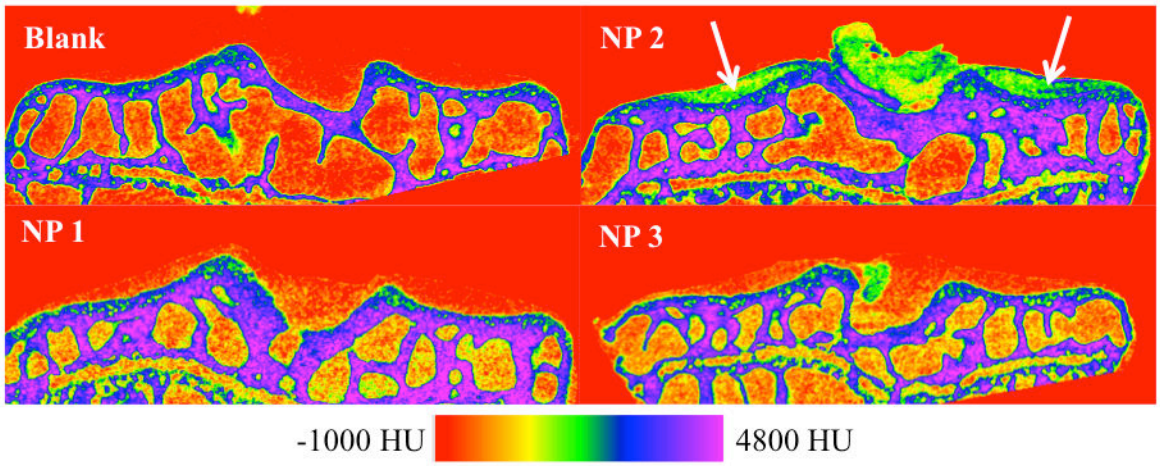

Figure 3.

2D coronal CT cross-sections of mouse tibia plateau articular cartilage after 48 hour exposure to NP contrast agents compared to a non-exposed (blank) specimen (6 μm resolution). NP **2** shows clear visualization of cartilage on the lateral and medial tibial plateaus (white arrows) as well as some midline remnant soft tissue ligaments that have also been shown to possess GAG content. NPs **1** and **3** uptake poorly into the articular cartilage and it is difficult to differentiate between air and cartilage in the image reconstructions.

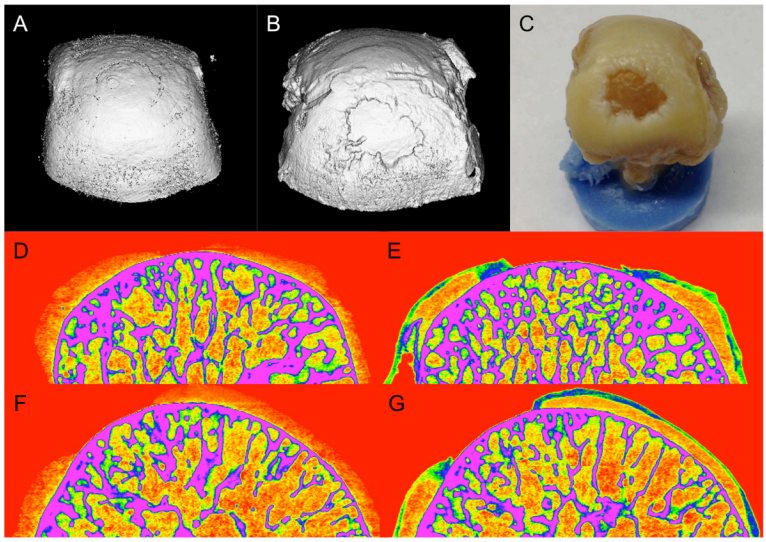

Figure 4.

Cartilage defect in the proximal metacarpal phalangeal (MCP) joint of a human index finger is clearly visualized only in the presence of NP **2**. The MCP was imaged before (A,D,F) and after (B,E,G) immersion in 40 mg NP/mL NP **2** for 24 hours. 3D CT reconstruction (B) shows the defect and is similar to that seen with gross inspection (C). Coronal (D&E) and sagittal (F&G) cross section 2D CT reconstructions are also shown which further document the requirement of using NP **2** to visualize the cartilage and the defect in the MCP.

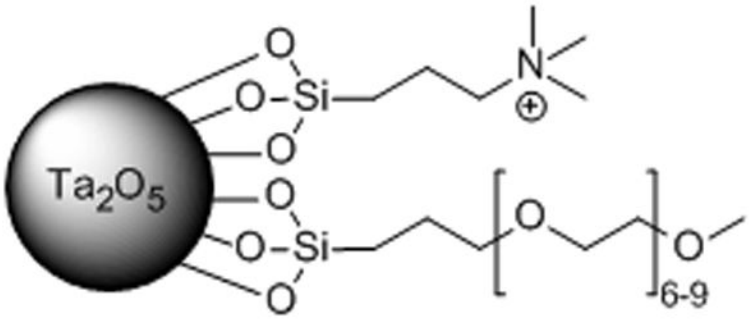

Figure 5.
Tantalum oxide NP with tetra-ammonium and (short) PEG ligands (NP **4**).

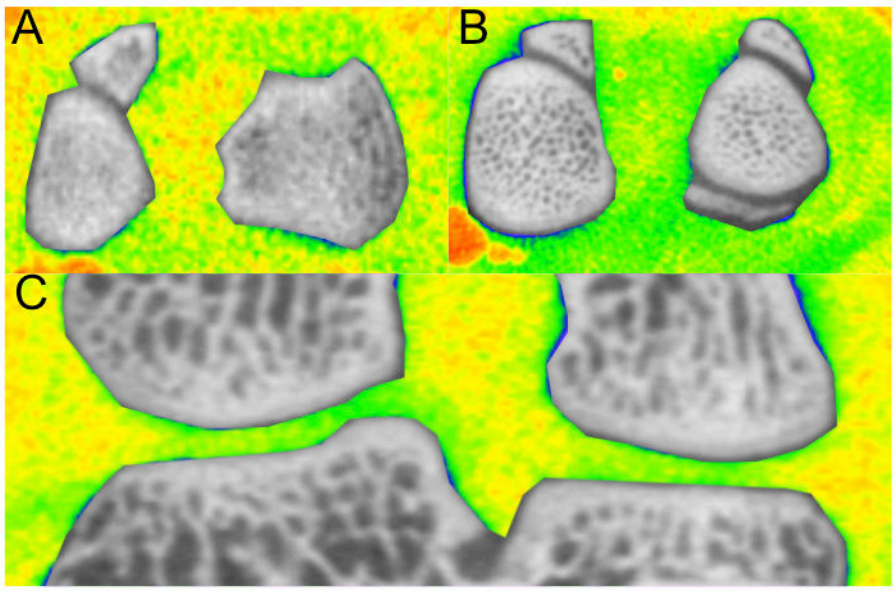

Figure 6.

A composite *in vivo* image (A) and *ex vivo* (B,C) showing the joint space in color and the bone in grayscale. Contrast (green) can be seen throughout the joint compared to soft tissue, highlighting the cartilage (A, B) or cartilage, tendon, and meniscus (C). The original, grayscale images can be found in the SI.

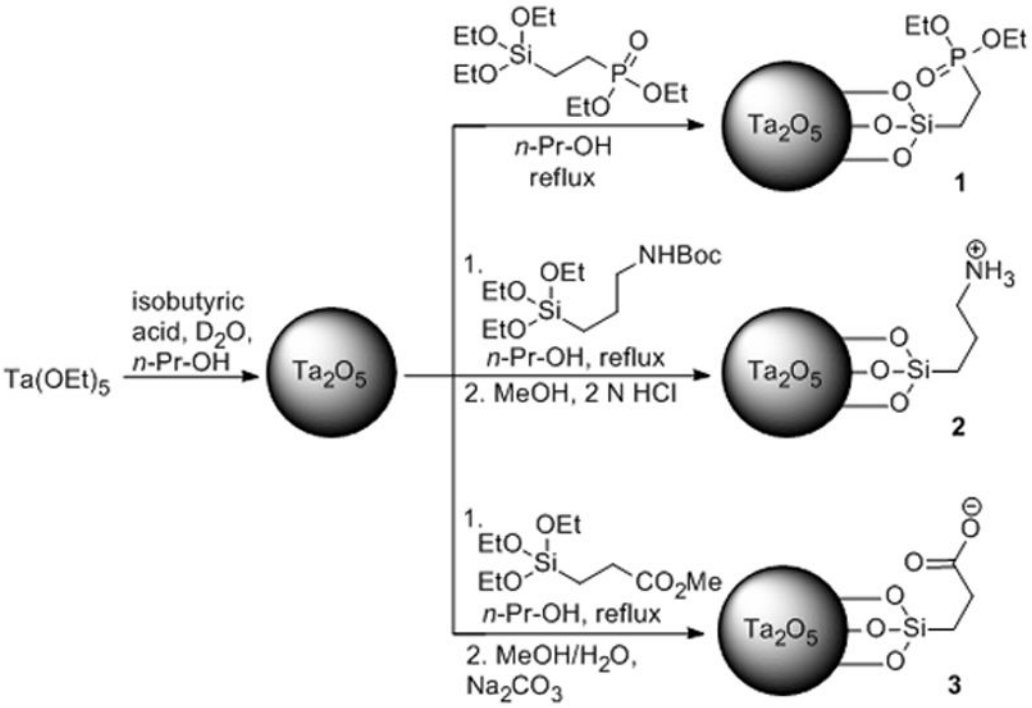

Scheme 1.

Synthesis of Ta_2O_5 NPs with neutral phosphonate (NP **1**), cationic ammonium (NP **2**) and anionic carboxylate (NP **3**) ligands at physiological pH.